Available online at www.sciencedirect.com

SCIENCE DIRECT®

Thin Solid Films 472 (2005) 64–70

thin solid films

www.elsevier.com/locate/tsf

Structural and microtribological studies of Ti–C–N based nanocomposite coatings prepared by reactive sputtering

D. Martínez-Martínez[a], J.C. Sánchez-López[a,*], T.C. Rojas[a]
A. Fernández[a], P. Eaton[b], M. Belin[c]

[a]*Instituto de Ciencia de Materiales de Sevilla (CSIC-Univ. de Sevilla), Avda, Americo Vespucio, s/n, Sevilla 41092, Spain*
[b]*Instituto de Investigaciones Químicas (CSIC-Univ. de Sevilla), Spain*
[c]*Ecole Centrale de Lyon, LTDS, France*

Received 20 May 2004; received in revised form 25 May 2004; accepted 7 June 2004
Available online 7 August 2004

Abstract

Ti–C–N thin films were synthesized at near room temperature by reactive magnetron sputtering of titanium and graphite targets in Ar or Ar/N_2 mixtures. The microstructure and chemical composition of the coatings were studied by transmission electron microscopy, atomic force microscopy (AFM), electron diffraction, X-ray diffraction, X-ray photoelectron spectroscopy and electron energy loss spectroscopy. For a pure Ar atmosphere, a microstructure constituted by small grains (10–20 nm) of a TiC phase encapsulated into an amorphous matrix is observed. AFM lateral force mapping shows a strong frictional contrast between the two phases. When nitrogen is introduced in the gas phase during preparation, the granular microstructure is not seen and the chemical composition is enriched in amorphous nonstoichiometric CN_x phases (a-CN_x) with different content of nitrogen ($0.5 \leq x \leq 0.7$). The type of structure and chemical bonding of the Ti–C–N films are correlated with the tribological properties at the microscopic level in order to establish the synthesis conditions leading to the nanocomposite formation.

Keywords: Titanium carbide; Atomic force microscopy (AFM); Electron energy loss spectroscopy (EELS); Tribology

1. Introduction

Hard thin film coatings find a widespread range of applications in many industrial processes that involve casting, forming or cutting tools due to the benefit in efficiency enhancement, tool lifetime before repairing and substitution and cost reduction. However, practical applications are limited to the use of lubricants helping to dissipate the energy, decrease friction coefficient as well as the risk of delamination or failure. Recent reports have shown that nanocomposites can reach very high hardness values (40–70 GPa) owing to the combination of a nanocrystalline phase of a hard compound (typically nitrides or carbides of transition metals) inside an amorphous matrix [1,2]. For tribological applications, e.g., bearing balls and gears, novel wear-resistant materials have been developed, which combine nanocrystalline carbides (TiC, WC), dichalcogenides (MoS_2, WS_2) and amorphous diamond-like carbon into nanocomposite structures [3,4]. The election of a low-friction-coefficient material as amorphous phase surrounding the nanocrystals may succeed in reducing the friction coefficient and the risk of brittle failure of the composite. In this work, the development of Ti–C–N based nanocomposite coatings is explored by reactive magnetron sputtering with Ar or Ar/N_2 mixtures of Ti and C targets. Their microstructure, chemical composition and bonding are discussed depending on the deposition conditions. The measurement of the local lateral forces over the sample surface will describe the coatings in terms of frictional aspects at the microscale.

* Corresponding author. Tel.: +34 95 448 9579; fax: +34 95 446 0665.
E-mail address: jcslopez@icmse.csic.es (J.C. Sánchez-López).

0040-6090/$ - see front matter © 2004 Elsevier B.V. All rights reserved.
doi:10.1016/j.tsf.2004.06.140

2. Experimental details

Ti–C–N coatings were prepared on AISI M2 polished steel and Si (100) substrates by reactive sputtering of titanium (Goodfellow, 99.99% purity) and graphite (Goodfellow, 99.9995% purity) targets in Ar and/or N_2 discharges. The sputtering conditions were 160 W, in r.f. mode, for the graphite target and 40 W, in d.c. mode, for the titanium target. The pressure of the vacuum chamber was measured before deposition in 6.5×10^{-4} Pa and about 7.5 Pa while growing. The substrates were mounted in a rotary sample holder (10 rpm) to ensure the homogeneity of the coatings and the temperature was determined in 75–85 °C during deposition by a chromel–alumel thermocouple. There was no additional substrate heating or biasing during deposition. The growth time was 120 min and the film thickness ranges from 0.1 to 0.5 μm.

The X-ray photoelectron spectroscopy (XPS) equipment is a VG-Escalab 210 Spectrometer working in the constant analyzer energy mode with a pass energy of 50 eV and nonmonochromatic Mg K_α radiation as excitation source. The binding energy reference was taken as the main component of the C 1s peak at 284.6 eV for a mixture of adventitious and pure carbon. For quantification, the XPS spectra were subjected to background subtraction (Shirley background) and sensitivity factors supplied by the instrument manufacturer were used.

Transmission electron microscopy (TEM), electron diffraction (ED) and electron energy loss spectroscopy (EELS) analyses were carried out in a Philips CM200 microscope operating at 200 kV and equipped with a parallel detection EELS spectrometer from Gatan (766-2 kV). For their observation, the films were grown on NaCl substrates and then floated off in water and supported on a holey carbon grid. The C, N, O and Ti core-loss edges were recorded in the diffraction mode with a camera length of 470 mm. Using a 2-mm spectrometer, entrance aperture yielded an energy resolution at the zero-loss peak of 1.4 eV. Spectra were recorded for dark current and channel-to-channel gain variation. Low-loss spectra were also recorded in the same illumination area (≈1 μm in diameter). Commercial TiC, TiN and TiO_2 powders, and an amorphous carbon nitride film (a-CN_x), described elsewhere [5], were measured in the same conditions to be used as reference compounds. After subtraction of the background by a standard power-law function, the spectra were deconvoluted for plural scattering with the Fourier-ratio method and normalized to the jump. All of these treatments were performed within the EL/P program (Gatan).

X-ray diffraction (XRD) diffractograms were carried out using CuK_α radiation in a Siemens D5000 diffractometer at an incidence angle of 1°.

Atomic force microscopy (AFM) measurements were carried out with a Topometrix Explorer (Veeco Instruments). Both topography and friction measurements were made in contact mode at applied load of ca. 2 nN. Rectangular silicon cantilevers (from Mikromasch, Estonia) with nominal tip radius of ≤10 nm and normal force constants of approximately 0.03–0.08 N/m were used. It was noted that the results obtained depend strongly on the tip condition. Therefore, brand new tips were used for each sample. Topography images have been shaded to enhance contrast. For measurement of friction force images (FFM), topographical effects (e.g., high apparent friction where the tip moves up a slope on the sample) must be removed from the lateral force images. In order to do this, friction images were obtained by subtracting reverse lateral force images from forward lateral force images after offset correction. This led to deflection images, which are proportional to friction.

3. Results and discussion

Table 1 summarizes the synthesis conditions for the coatings under study and the atomic chemical composition determined by XPS and EELS techniques. Fig. 1 plots the variation of the atomic percentages measured by XPS versus the fraction of nitrogen flow in the Ar/N_2 mixture used during the deposition. In general, a low quantity of titanium is incorporated in the films, especially when N_2 is used as sputtering gas. The oxygen contamination is not negligible and it varies in a parallel way with the titanium concentration, pointing out this element as main agent of oxygen trapping. Simultaneously, an increase of nitrogen and carbon contents is observed as the nitrogen flow rises. Further chemical and structural characterization has been carried out on three selected samples C1 (100% Ar), C2 (25% N_2) and C5 (100% N_2) as representative examples of the different regions depicted in the plot. The composition of these films estimated by quantitative EELS (Table 1) gave higher Ti and N contents than XPS due to the surface-sensitive character of this last technique and the presence of

Table 1
Summary table of synthesis conditions and chemical compositions obtained by quantitative XPS and EELS for the Ti–C–N based coatings

Sample	Synthesis	XPS (at.%)					EELS (at.%)				
		Ti	C	N	O	N/C	Ti	C	N	O	N/C
C1	100% Ar	17	43	2	38	<0.1	51	34	0	15	0
C2	25% N_2+75% Ar	2	58	28	12	0.5	7	43	45	5	1.0
C3	50% N_2+50% Ar	1	59	30	10	0.5	not measured				
C4	75% N_2+25% Ar	<1	60	30	10	0.5	not measured				
C5	100% N_2	<1	70	17	13	0.2	3	49	45	3	0.9

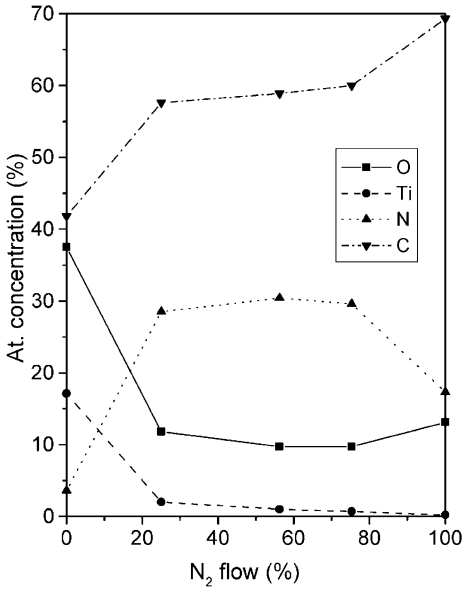

Fig. 1. Changes in the relative atomic percentages measured by XPS as a function of the nitrogen % in the inlet-gas flow.

adventitious carbon at the surface. Oxygen contamination reached a maximum of 14.8% for the highest Ti concentration owing to the reactive nature of titanium and reduced appreciably, 3.2% for the sample C5, with decreasing Ti incorporation. Nevertheless, oxygen-containing Ti–C–N coatings and disordered forms of TiO_2 (usually known as "Magnéli oxides") have also been presented as good prospects for anti-wear applications [6–8].

The different film microstructures observed by TEM are illustrated in Fig. 2 together with their associated electron diffraction patterns. The sample C1 (Fig. 2a), prepared with 100% Ar in the gas phase, shows a singular microstructure composed by small crystals (10–20 nm) uniformly distributed in an amorphous matrix, while the other two exhibit a homogeneous structure with no crystalline patterns. It is worth mentioning that the different islands (100–200 nm across) observed in the micrographs Fig. 2b and c could be attributed to the growth of the films on top of the terraces of NaCl substrates. The electron diffraction pattern from C1 exhibits rings originated by a polycrystalline phase, while in samples C2 and C5, only a diffuse halo is noticed due to the

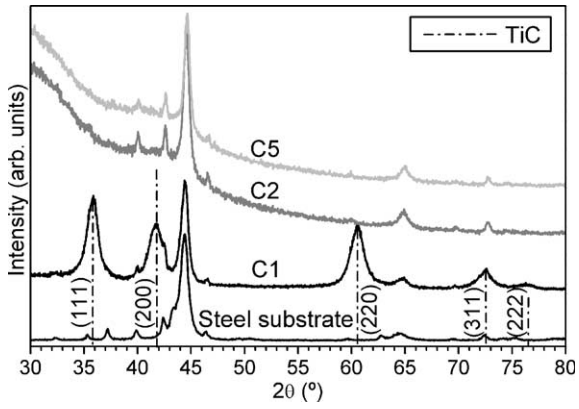

Fig. 3. Grazing angle XRD diffractograms of the C1, C2 and C5 coatings deposited onto steel substrates at 1° incidence angle. The XRD diagram of the steel substrate is also included for comparison purposes. The broken vertical lines indicate the positions of the diffraction peaks for a TiC phase.

amorphous nature of these films. In the diffraction pattern of C1 sample, the (111) and (200) TiC planes can be identified, very close to each other, with d-spacing of 0.25 and 0.22 nm, respectively. The third brightest ring is originated by the (220) TiC planes with a 0.15 nm d-spacing.

X-ray diffraction analyses of the three coatings at grazing angle of 1° (Fig. 3) show that the C1 sample contains a nanocrystalline TiC phase, whereas in the other two coatings, only the peaks from the steel substrate are observed. In addition, we have estimated from the broadening of the TiC peaks and the Scherrer formula an average crystallite size of 10 nm for the C1 sample in quite good agreement with the TEM observation. No evidences of crystalline titanium oxides are detected, indicating that these phases if present must be amorphous.

The type of chemical bonding was investigated by XPS and EELS analysis. Fig. 4 displays the C 1s, N 1s and Ti 2p photoelectron peaks for the three selected coatings. In the first approximation, the spectra are obtained directly from the film surface without previous surface cleaning with Ar^+ bombardment. The Ti 2p photoelectron peak is characterized by two distinct components (Fig. 4a). The one exhibiting the Ti $2p_{3/2}$ peak at 455.0 eV of binding energy (B.E.) is assigned to TiC species and the other at 458.5 eV to TiO_2. The C 1s

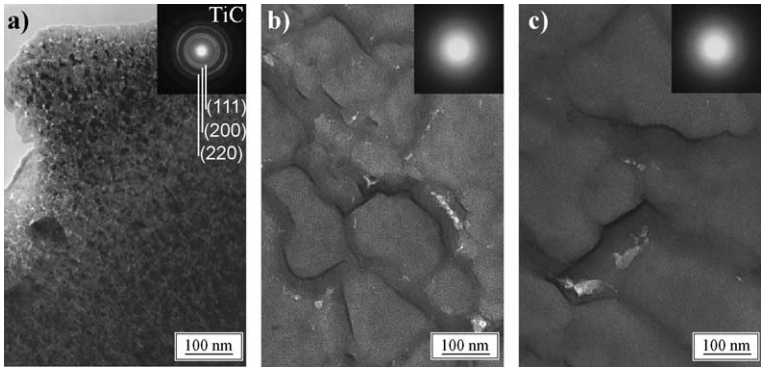

Fig. 2. TEM micrographs and selected area diffraction patterns for C1 (a), C2 (b) and C5 (c) coatings.

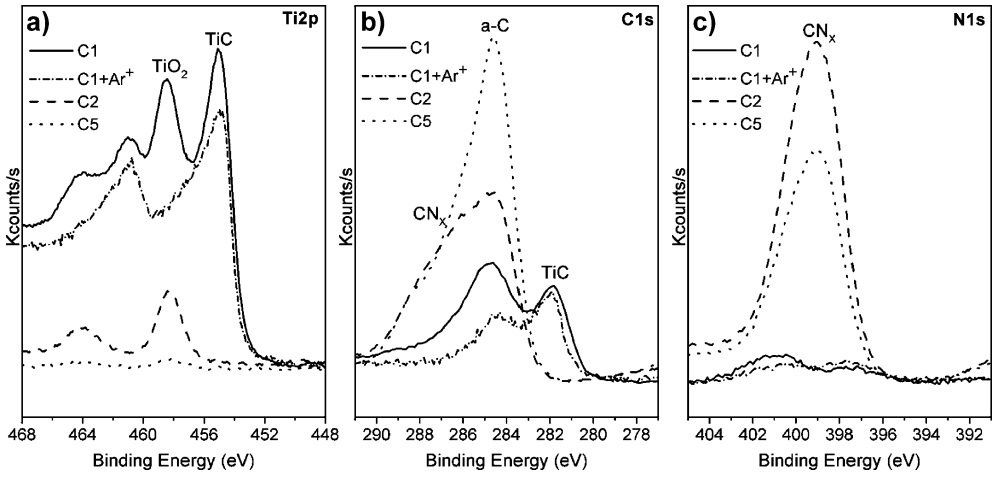

Fig. 4. Ti 2p, C 1s and N 1s photoelectron peaks obtained for the C1, C2 and C5 coatings. The same spectra for the C1 sample after 30 s of Ar^+ sputtering are also included for comparison purposes.

peak, shown in Fig. 4b, is composed of several components with different chemical shifts. The main component at 284.6 eV can be assigned to a mixture of carbon in C−C bonds and adventitious hydrocarbons. This peak shows an asymmetric broadening towards higher binding energies (≈286–288 eV). This effect has been widely observed in the deposition of a-CN_x films [9,10] and attributed to sp^2 hybridized-C bonded to N in two different environments. The peak with lowest B.E. (281.5 eV) is assigned to TiC species in agreement with previous works [11]. The contribution of these chemical bondings differs significantly depending on the synthesis conditions. Thus, the coating C1, prepared with 100% Ar in the gas phase, is characterized by the apparition of carbides species, while in the samples C2 and C5, the Ar/N_2 mixtures produced a significant formation of CN_x compounds. Accordingly to Ref. [10], we have deconvoluted the C−N bonding into two components: C twofold coordinated to N at 285.9 eV and C threefold coordinated to N at 287.7 eV, respectively. The calculation of the C–N contribution to the total C 1s signal allows to estimate the nitrogen content in the a-CN_x films, giving x values of 0.5 for sample C5 and 0.7 for samples C2, C3 and C4, respectively. In sample C1, in order to discriminate the contribution of the amorphous carbon phase from the adventitious carbon, a surface bombardment with Ar^+ ions (3.5 keV) was performed during 30 s (see C1+Ar^+ curves in Fig. 4). After the sputtering cleaning, two peaks can be clearly distinguished in the C 1s photoelectron peaks at 284.0 and 281.5 eV corresponding to C bonded to carbon (a-C) and Ti (TiC), respectively. The Ti 2p spectrum recorded in the same conditions exhibits a main peak at 455.0 eV assigned to TiC, whereas the component due to TiO_2 is absent, which implies that carbon signal at 284.0 eV is therefore mainly due to the film composition and not from the adventitious contamination. The broadening of the TiC peak is explained by the presence of different types of Ti−O bonds, as TiO (455.1 eV) and Ti_2O_3 (457.8 eV) [12]. By quantification of the peak areas of C 1s components owing to a-C and TiC phases, the percentages were estimated to be 45% and 55%, respectively.

The N 1s peak (Fig. 3c) for the coatings C2 and C5 present a broad peak centered around 399 eV. A low N concentration (≈2%) is noticed for C1 coating due to nitrogen impurities in the sputtering targets. The existence of N−Ti bonds results in a N 1s photoelectron peak around 396.5 eV. Instead of that, the position of the N 1s peak is in agreement with N bonded to C in sp^2 domains, as demonstrated in a previous work [10]. The carbon contents for these samples increased up to 60–70 at.%, while the titanium concentration diminishes significantly. All this suggests that N_2 discharges lead to a preferential sputtering of the C target and the subsequent formation of a-CN_x phases instead of titanium nitride. Nevertheless, in order to obtain further information concerning the chemical bonding inside the Ti–C–N films, we have used EELS spectra collected for the same representative samples C1, C2 and C5.

In Fig. 5, the Ti $L_{2,3}$-edge, C K-edge and the low-loss spectra for the three coatings are displayed, ordered by increased N/C ratio, together with reference edges measured from TiO_2, TiC and a-CN_x standards. The comparison of the near-edge fine structure (ELNES) of the ionization edges (Ti and C) for the samples with those of the references allows to differentiate two types of behavior. Thus, the Ti $L_{2,3}$-ionization edge for the C1 coating presents very similar features to that obtained for the TiC reference. However, in the coatings C2 and C5, the spin-orbit splitting between L_2 and L_3 increases as occurs in the TiO_2 standard due to the shift of the L_3 edge at lower values (454.5 eV). These differences are further confirmed in the variation of the C K-edge (Fig. 5b). The C K core-loss spectrum for an amorphous CN_x described in a previous work is included for comparison purposes [5]. The ELNES of TiC is dominated by well-

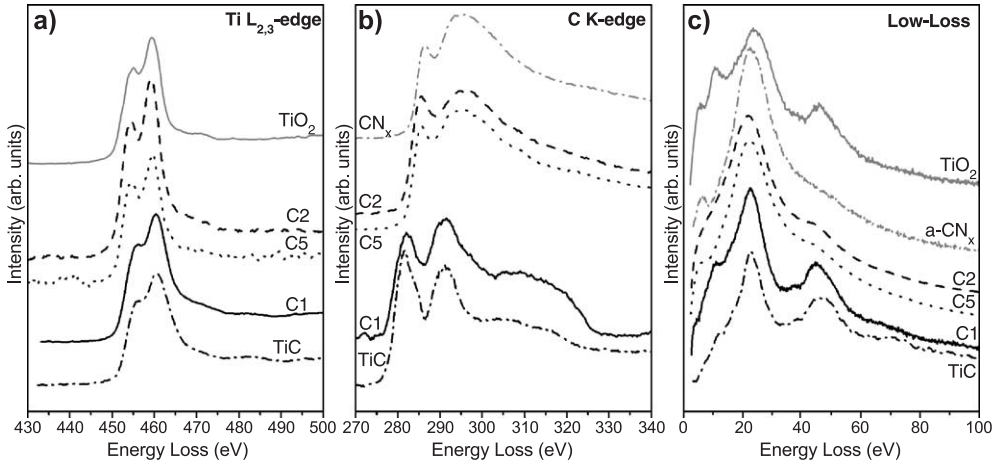

Fig. 5. Ti $L_{2,3}$-edge (a), C K-edge (b) and low-loss (c) electron energy loss spectra for the C1, C2 and C5 coatings. TiC, TiO_2 and a-CN_x references are included for comparison purposes.

separated strong π and σ peaks of approximately equal intensity centered at ≈283 and 292 eV, respectively. Metal–nonmetal bonds in cubic refractory compounds are formed in two ways: a σ bond, i.e. an overlap of nonmetal 2p and metal 3d-e_g sites, and π-bond, i.e. an overlap of the nonmetal 2p with the metal 3d-t_{2g} orbitals [13]. The overall shape and position for sample C1 appear to be similar to those of TiC phase, although some broadening and changes in intensity are due to the presence of amorphous carbon. For the remaining samples, the position of the C K-edges at 285.6 eV and the intensity of the π peak are similar to those reported in amorphous CN_x films [5,14] prepared by different techniques. The low-loss regions for the studied samples are depicted in Fig. 5c compared to those obtained for TiC, TiO_2 and a-CN_x references. The most prominent feature appears at 23–24 eV corresponding to the bulk plasmons. At energies above 30 eV, the spectra of TiC and TiO_2 show a second broad peak centered around 46 eV that corresponds to excitations from the Ti 3p level [15]. The overall shape and peak positions for the C1 sample agrees quite well with TiC standard though a certain contribution of titanium oxide can be inferred from the changes in the 46-eV peak. The low-loss regions for the remaining samples C2 and C5 are very similar to those obtained from an amorphous CN_x film with a small shoulder at ≈44 eV due to a certain contribution of the titanium oxide.

In summary, the characterization performed in the Ti–C–N systems by TEM/EELS, ED, XRD and XPS techniques suggests the formation of nanocrystalline TiC particles with an average diameter of 10–20 nm for C1 coating embedded in a disordered carbon and titanium oxide matrix, whereas the nitrogen incorporation (samples C2 and C5) leads to an amorphous multiphase consisting of CN_x, C and a small amount of titanium oxide.

In past studies, the nanocrystalline-amorphous carbon composites have been obtained by reactive sputtering deposition at relatively high substrate temperature (500–600 °C) [16] or combined with high-energy plumes from laser ablation technique [17] to promote the growth of a crystallite phase. More recently, Feng et al. [18] have demonstrated the precipitation of TiC nanoclusters within a-C and a-C:H structures using an industrial scale, four cathode, unbalanced magnetron sputtering system, at Ti compositions >8 at.%. Other authors have combined physical and chemical vapor deposition processes to reach higher plasma densities than conventional magnetron sputtering [19,20]. The double magnetron reactive sputtering process used in this study enables the deposition of the nanocomposites at temperatures even below 80 °C, without biasing the substrate.

The observation of the coatings by scanning force microscopy helps to understand their particular microstructure and their influence on the friction properties by measuring the vertical and lateral deflection of the cantilever while the sample surface is scanned. The advantages of this approach are illustrated in Fig. 6 by comparing the behavior of the tip moving on C1 and C2 coatings. Two-dimensional profiles of surface height and friction forces data in trace and retrace directions are also included. The sample textures (Fig. 6a and c) are characterized by round agglomerates with sizes ranging between 20 and 30 nm. The average surface roughness are estimated to be 2.43±0.55, 1.98±0.51 and 2.31±0.43 nm for the C1, C2 and C5 coatings, respectively. Local variations in the microscale friction are observed for the C1 friction force mapping between the grains and the boundary region (Fig. 6b), whereas the analogous image obtained for C2 does not show a well-expressed friction contrast (Fig. 6d). Nevertheless, Sundarajan and Bhushan [21] noted that subtraction of reverse lateral forces from forward lateral forces does not remove topographic effects entirely, especially when imaging high aspect ratio features. The examination of back and forth profiles is useful in understanding the origins of the observed

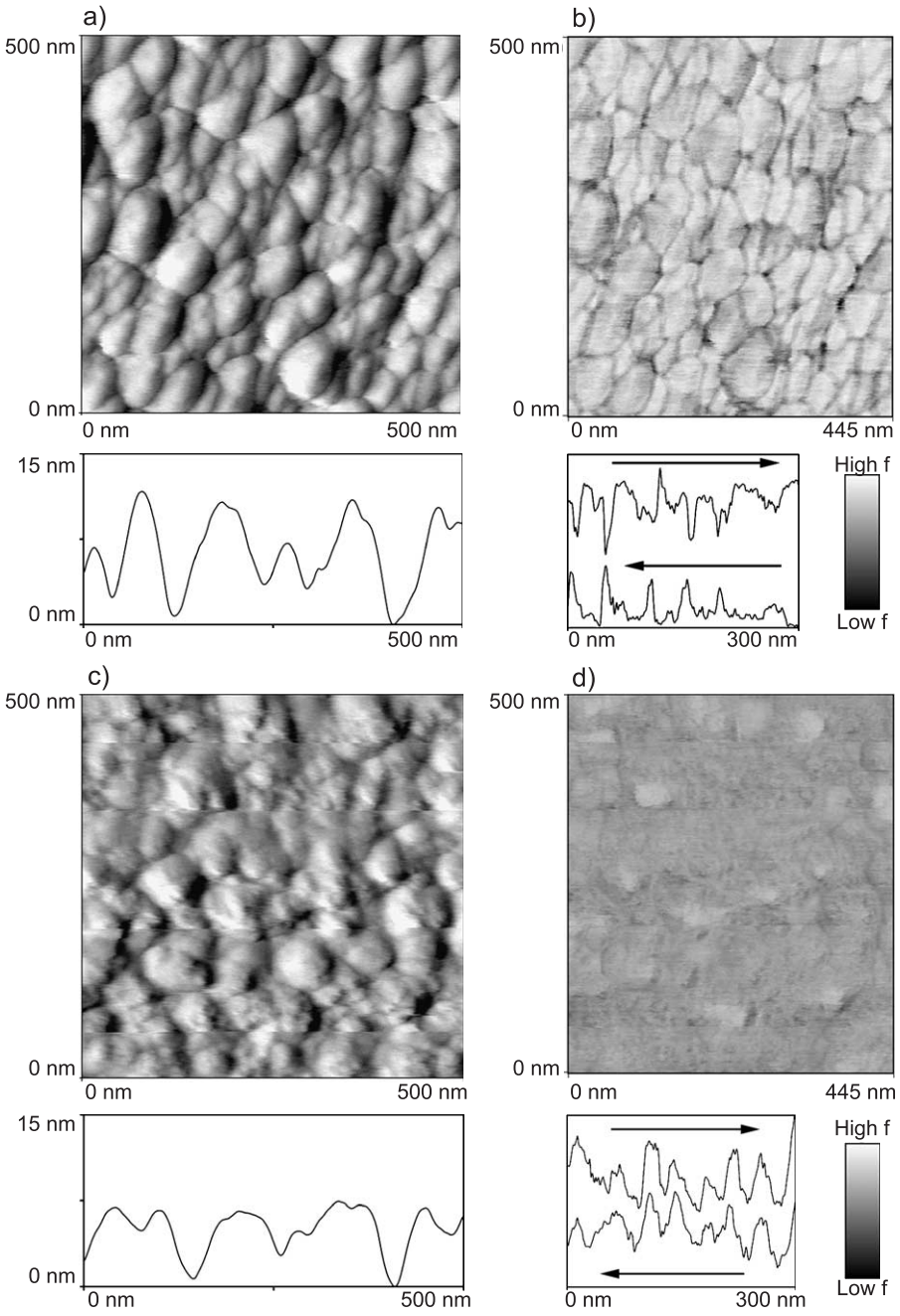

Fig. 6. Surface topography map and associated line profiles taken for C1 (a) and C2 (c) coatings. Friction force maps and tip lateral deflections in forward and reversed directions for C1 (b) and C2 (d) samples. Higher points are shown by lighter contrast.

friction forces in both samples. The lateral forces for C2 present similar trend in both profiles, indicating that this variation is exclusively related to topographical effects. However, in C1 sample, there is an additional component in friction force that does not depend on the scan direction. Many of the maximum peaks in the forward scan coincide with minimum values in the reversed scan. Thus, the local friction variations between both films arise from the different structure and crystallinity. Differences in friction have also been observed for multiphase ceramic materials [22]. TEM and diffraction techniques proved the existence of a polycrystalline TiC phase dispersed in an amorphous matrix only for the film prepared in 100% Ar (C1). Therefore, a higher torsion of the cantilever is expected at the top of the TiC grains (hard phase) in respect to the boundary region (soft phase). The lack of frictional contrast in the remaining samples is in agreement with a homogeneous distribution in chemical bondings and structure as previously stated. By this method, it is possible to distinguish areas of different chemical composition and/or structure in multiphase nanocomposite coatings.

4. Summary and conclusions

In this work, the formation of Ti–C–N nanocomposite coatings based on nanocrystals of a hard phase (TiN or TiC) embedded in a lubricant phase (a-C or a-CN_x) was pursued by varying the N_2/Ar ratio in a double magnetron sputtering system. This particular microstructure was revealed by TEM and AFM techniques for the TiC/a-C nanocomposite prepared with 100% Ar in the plasma discharge at near room temperature. Over the studied N_2/Ar mixtures, a preferential sputtering of the carbon target by the N_2^+ and N^+ ions led to the formation of amorphous carbon nitride phases mixed with titanium oxides instead of the searched chemical and microstructural composition. XPS and EELS techniques provided further evidences of the different chemical bonding found in the films depending on the nitrogen incorporation. Local variations in the friction maps were observed for the coating prepared in pure Ar revealing the hybrid nature (nanocrystalline/amorphous) of this nanocomposite. All these results suggest that a conventional magnetron sputtering system results valid for the synthesis of TiC/amorphous C-based nanocomposite materials. Finally, AFM/FFM measurements are presented as a suitable tool for the structural and tribological characterization of nanocomposite materials. Further experiments are necessary to achieve a better understanding of the frictional properties at the microscale and their comparison to the macroscale behavior by means of microindentation and conventional tribological tests.

Acknowledgements

This work has been funded by the Spanish MCYT (project no. MAT2001-1399-C02-01 and Ramón y Cajal Program). We are especially grateful to Mrs. I. Rosa and Mr. J.C. Millán for technical support.

References

[1] P. Nesládek, S. Vepřek, Phys. Status Solidi, A 177 (2000) 53.
[2] S. Vepřek, J. Vac. Sci. Technol., A 17 (1999) 2401.
[3] A.A. Voevodin, J.S. Zabinski, Thin Solid Films 370 (2000) 223.
[4] A. Savan, E. Pflüger, R. Goller, W. Gissler, Surf. Coat. Technol. 126 (2000) 159.
[5] J.C. Sánchez-López, C. Donnet, M. Belin, T. Le Mogne, C. Fernández-Ramos, M.J. Sayagués, A. Fernández, Surf. Coat. Technol. 133–134 (2000) 430.
[6] J.H. Hsieh, W. Wu, C. Li, C.H. Yu, B.H. Tan, Surf. Coat. Technol. 163–164 (2003) 233.
[7] M. Woydt, Tribol. Lett. 8 (2000) 117.
[8] O. Storz, H. Gasthuber, M. Woydt, Surf. Coat. Technol. 140 (2001) 76–81.
[9] J.C. Sánchez-López, C. Donnet, F. Lefebvre, C. Fernández-Ramos, A. Fernández, J. Appl. Phys. 90 (2001) 675.
[10] A. Fernández, C. Fernández-Ramos, J.C. Sánchez-López, Surf. Coat. Technol. 163–164 (2003) 527.
[11] A.A. Voevodin, J.S. Zabinski, J. Mater. Sci. 33 (1998) 319.
[12] K. Baba, R. Hatada, Surf. Coat. Technol. 136 (2001) 192.
[13] J. Pflüger, J. Fink, G. Crecelius, K.P. Bohnen, H. Winter, Solid State Commun. 44 (1982) 489.
[14] L. Wan, R.F. Egerton, Thin Solid Films 279 (1996) 34.
[15] G.G. Fuentes, I.G. Mancheño, F. Balbás, C. Quirós, J.F. Trigo, F. Yubero, E. Elizalde, J.M. Sanz, Phys. Status Solidi, A 175 (1999) 429.
[16] S. Vepřek, M. Haussmann, S. Reiprich, J. Vac. Sci. Technol., A 14 (1996) 46.
[17] A.A. Voevodin, S.V. Prasad, J.S. Zabinski, J. Appl. Phys. 82 (1997) 855.
[18] B. Feng, D.M. Cao, W.J. Meng, J. Xu, R.C. Tittsworth, L.E. Rehn, P.M. Baldo, G.L. Doll, Surf. Coat. Technol. 148 (2001) 153.
[19] T. Zehnder, J. Patscheider, Surf. Coat. Technol. 133–134 (2000) 138.
[20] W.J. Meng, R.C. Tittsworth, L.E. Rehn, Thin Solid Films 377–378 (2000) 222.
[21] S. Sundarajan, B. Bhushan, J. Appl. Phys. 88 (2000) 4825.
[22] V.N. Koinkar, B. Bhushan, Wear 202 (1996) 110.